

How disorder affects the Berry-phase anomalous Hall conductivity: the view from k space

Raffaello Bianco,^{1,2} Raffaele Resta,^{1,3} and Ivo Souza^{2,4}

¹*Dipartimento di Fisica, Università di Trieste, 34127 Trieste, Italy*

²*Centro de Física de Materiales, Universidad del País Vasco, 20018 San Sebastián, Spain*

³*Donostia International Physics Center, 20018 San Sebastián, Spain*

⁴*Ikerbasque Foundation, 48011 Bilbao, Spain*

(Dated: June 20, 2021)

The anomalous Hall conductivity of “dirty” ferromagnetic metals is dominated by a Berry-phase contribution which is usually interpreted as an intrinsic property of the Bloch electrons in the pristine crystal. In this work we evaluate the geometric Hall current directly from the electronic ground state with disorder, and then recast it as an integral over the crystalline Brillouin zone. The integrand is a generalized k -space Berry curvature, obtained by unfolding the Berry curvature from the small Brillouin zone of a large supercell. Therein, disorder yields a net extrinsic Hall contribution, which we argue is related to the elusive side-jump effect. As an example, we unfold the first-principles Berry curvature of an Fe₃Co ordered alloy from the original fcc-lattice Brillouin zone onto a bcc-lattice zone with four times the volume. Comparison with the virtual-crystal Berry curvature clearly reveals the symmetry-breaking effects of the substitutional Co atoms.

I. INTRODUCTION

The anomalous Hall effect (AHE) in metallic ferromagnets includes a purely geometric bandstructure contribution given by the k -space Berry curvature of the occupied Bloch states.^{1,2} Somewhat counterintuitively, this *intrinsic* contribution only becomes dominant in moderately resistive (“dirty”) samples, for which crystal momentum is not a good quantum number and the Berry curvature strictly speaking is ill-defined. In highly-conducting pristine samples with sharply defined energy bands and Berry curvature, the AHE is instead dominated by an *extrinsic* contribution, skew-scattering from dilute impurities.^{1,2}

Motivated by these considerations, we introduce a generalized k -space Berry curvature for metallic systems with disorder. Integrated over the Brillouin zone (BZ) of the underlying ordered cell it gives the dominant contribution to the anomalous Hall conductivity (AHC), expressed as a property of the disordered electronic ground state. We will call this the *geometric* AHC contribution. It combines the nominally intrinsic contribution with certain disorder effects of a similar nature. With this definition we depart from the standard terminology, where the words “intrinsic” and “geometric” (or “Berry-phase”) are used interchangeably when referring to AHC contributions.^{1,2} The proposed definition has the merit of being directly applicable to the experimental regime of interest, where scattering from disorder is important.

Our generalized Berry-curvature definition is based on the notion of BZ unfolding, which has been used extensively in recent years in the context of band structure calculations with periodic supercells.^{3–5} Similar unfolding techniques were introduced long ago to describe the phonon spectra of disordered alloys.⁶

Unfolding band structures of supercell (SC) calculations is a particularly informative way of visualizing the

influence of impurities (or other sources of broken translational order) on the electronic states in crystals. For weak to moderate disorder the unfolded bands resemble those of the pristine crystal, with the deviations in both the dispersion and the spectral weight reflecting the effect of the disorder potential.³ The recent development of efficient *ab-initio*-based SC methodologies⁷ opens up new possibilities for applying unfolding techniques to large SCs with realistic descriptions of disorder.^{8,9}

So far, BZ unfolding has been used mainly to extract approximate energy dispersions for disordered systems. While the energy bands $\epsilon_{\mathbf{k}i}$ are the most basic quantity in the theory of solids, it is now understood that the k -space Berry curvature $\Omega_i(\mathbf{k}) = \nabla_{\mathbf{k}} \times \mathbf{A}_i(\mathbf{k})$ is an additional fundamental ingredient determining the dynamics of electrons in crystals.² (Here $\mathbf{A}_i(\mathbf{k})$ is the Berry connection, to be defined shortly.) Using Stokes’ theorem, the Berry curvature can be viewed as the geometric phase $\varphi_i = \oint \mathbf{A}_i(\mathbf{k}) \cdot d\mathbf{l}$ per unit area picked up by a Bloch electron in band i as it is transported adiabatically along a small loop in k -space. The Berry curvature is generically nonzero in the BZ of crystals with broken inversion or time-reversal symmetry. It modifies the motion of electron wavepackets driven by an electric field \mathbf{E} , by adding a transverse “anomalous velocity” term $(e/\hbar)\Omega_i(\mathbf{k}) \times \mathbf{E}$ to the usual band velocity $(1/\hbar)\nabla_{\mathbf{k}}\epsilon_{\mathbf{k}j}$.

The intrinsic AHC is a direct consequence of the anomalous velocity. It is given by^{1,2}

$$\sigma_{ab}^{\text{int}} = -\frac{e^2}{h} \int_{\text{NBZ}} \frac{d^3k}{(2\pi)^3} \Omega_{ab}^{\text{occ}}(\mathbf{k}) \quad (1)$$

$$\Omega_{ab}^{\text{occ}}(\mathbf{k}) = \sum_i f_{\mathbf{k}i} \Omega_{i,ab}(\mathbf{k}) \quad (2)$$

$$\Omega_{i,ab}(\mathbf{k}) = \epsilon_{abc} \Omega_{i,c}(\mathbf{k}) = \nabla_{k_a} A_{i,b}(\mathbf{k}) - \nabla_{k_b} A_{i,a}(\mathbf{k}), \quad (3)$$

where $f_{\mathbf{k}i}$ is the occupation of the Bloch eigenstate $|\mathbf{k}i\rangle = e^{i\mathbf{k}\cdot\mathbf{r}}|u_{\mathbf{k}i}\rangle$ and $\mathbf{A}_i(\mathbf{k}) = i\langle u_{\mathbf{k}i}|\nabla_{\mathbf{k}}u_{\mathbf{k}i}\rangle$ is the Berry connection of the i -th band. The integral in Eq. (1) is over the BZ of the pristine crystal, which we will call the “normal Brillouin zone” (NBZ).

The definition of the intrinsic AHC as a Berry curvature in k space relies on perfect translational order. This is at odds with the above-mentioned fact that the intrinsic contribution tends to dominate in dirty samples with broken translational invariance. The conventional formulation becomes even more problematic for intrinsically disordered systems such as random alloys, for which there is no experimentally accessible “clean limit.” And yet, it is still useful to reason in terms of “intrinsic” contributions to the AHE in such moderately conducting systems.¹⁰

In view of these difficulties, how should the intrinsic AHC be defined and calculated in the presence of disorder? The standard procedure is to define it in terms of the Berry curvature of an ordered reference system – the pristine crystal in the case of doped samples,^{11,12} or a “virtual crystal” effective Hamiltonian in the case of alloys¹³ – calculated using the band filling appropriate to the doping level or alloying concentration. Disorder effects can be included via a diagonal self-energy term inserted in the energy denominator of the sum-over-states expression for the Berry curvature [Eq. (6) below], to account for the finite lifetime of the Bloch eigenstates.¹² A related strategy, which has been implemented within the coherent-potential approximation, is to compute the intrinsic AHC starting from the Kubo-Strěda equation, by combining all terms not connected to vertex corrections.¹⁰ While physically motivated, these remain somewhat *ad-hoc* and model-dependent prescriptions, which can only be justified for sufficiently dilute or concentrated alloys.

We propose a different approach, where we do not insist on defining precisely the intrinsic AHC contribution in a disordered system, and replace it with the geometric AHC. In the SC approach it is computed by inserting into Eq. (1) the electronic states of the SC system,

$$\sigma_{ab}^{\text{geom}} = -\frac{e^2}{h} \int_{\text{SBZ}} \frac{d^3K}{(2\pi)^3} \Omega_{ab}^{\text{occ}}(\mathbf{K}), \quad (4)$$

and averaging over several realizations of disorder. Here $\Omega_{ab}^{\text{occ}}(\mathbf{K})$ is the Berry curvature of the occupied SC eigenstates $|\mathbf{K}J\rangle$, and the integral is over the supercell Brillouin zone (SBZ). No phenomenological lifetime broadening parameter needs to be included in the Berry curvature calculation, since spectral broadening by disorder is already built-in, as revealed by the configuration-averaged unfolded energy bands.⁷⁻⁹

Equation (4) is a very plausible generalization of Eq. (1) in the context of SC calculations, where a disordered system is modeled as a “crystal” with a very large “primitive cell.” It correctly gives a quantized value for the AHC of 2D disordered Chern insulators when the Fermi level lies in the mobility gap,^{14,15} and we propose

to use it to unambiguously identify a dominant contribution to the AHC of *metallic* disordered systems. (Contrary to the case of Chern insulators, Eq. (4) does not capture the full AHC of a metal in a finite SC; we will return to this point in Sec. VI.)

Realistic descriptions of disorder require reasonably large SCs. The integration volume in Eq. (4) then becomes very small, and all k -space information is lost. In order to restore a k -space description reminiscent of Eq. (1), we recast Eq. (4) as the NBZ integral of a suitably defined “unfolded Berry curvature,”

$$\sigma_{ab}^{\text{geom}} = -\frac{e^2}{h} \int_{\text{NBZ}} \frac{d^3k}{(2\pi)^3} \Omega_{ab}^{\text{unf}}(\mathbf{k}). \quad (5)$$

Although with disorder present the unfolded curvature is no longer geometric in the strict sense (the interpretation as a Berry phase per unit area is lost), it remains gauge invariant in the NBZ. To illustrate its behavior in metallic systems with reduced translational order, we will implement Eq. (5) from first-principles, and apply it to a simple test case of an ordered magnetic alloy.

The manuscript is organized as follows. In Sec. II we motivate our approach starting from the Berry curvature defined in the folded BZ of a disordered SC. In Sec. III we introduce a general BZ unfolding formalism, which we then apply to the Berry curvature; the details of the implementation in a Wannier-function basis are also given. In Section V we compute from first-principles the unfolded curvature of an ordered Fe₃Co alloy, and compare it with the Berry curvatures of pure bcc Fe and of the alloy in the virtual-crystal approximation (VCA). We conclude in Section VI with a discussion and an outlook.

II. BERRY CURVATURE IN THE FOLDED BRILLOUIN ZONE

The formal connection between the geometric and linear-response formulations of the intrinsic AHC is provided by the spectral representation of Eq. (2),

$$\Omega_{ab}^{\text{occ}}(\mathbf{k}) = -\text{Im} \sum_{i,j} (f_{\mathbf{k}i} - f_{\mathbf{k}j}) \frac{\langle \mathbf{k}i | \hat{h} \hat{v}_a | \mathbf{k}j \rangle \langle \mathbf{k}j | \hat{h} \hat{v}_b | \mathbf{k}i \rangle}{(\epsilon_{\mathbf{k}j} - \epsilon_{\mathbf{k}i})^2}, \quad (6)$$

whose NBZ integral (1) is equivalent to the Kubo-Greenwood formula for the AHC in the clean limit.¹

Equation (6) is written in terms of the Bloch eigenstates and energy eigenvalues of a pristine crystal. If we place the crystal in a periodic SC and introduce some disorder, the disorder potential mixes states with different NBZ momenta \mathbf{k} and \mathbf{k}' whenever $\mathbf{k}' - \mathbf{k}$ equals a SC reciprocal vector \mathbf{G} , forcing the new eigenstates to be labeled by a common wavevector \mathbf{K} in the SBZ. The Berry curvature can still be defined in the SBZ from Eq. (6), now written in terms of the SC eigenstates $|\mathbf{K}J\rangle$, energy eigenvalues $\epsilon_{\mathbf{K}J}$, and occupations $f_{\mathbf{K}J}$.

Because of those extra couplings from disorder, it is not obvious how to map (unfold) the Berry curvature

from the SBZ onto the NBZ of the original crystal. Clearly, $\Omega^{\text{occ}}(\mathbf{K})$ is not simply equal to the virtual-crystal Berry curvature summed over the points $\{\mathbf{k}_s\}$ which fold onto \mathbf{K} : $\Omega^{\text{occ}}(\mathbf{K}) \neq \sum_s \Omega_{\text{VCA}}^{\text{occ}}(\mathbf{k}_s)$. Nevertheless, it will be possible to arrive at a unique definition for the unfolded Berry curvature with all the desired properties, namely: (i) it reduces to the ordinary Berry curvature $\Omega^{\text{occ}}(\mathbf{k})$ in the clean limit; (ii) it remains sharply defined (gauge-invariant) in the presence of disorder; and (iii) it constitutes a proper mapping from the SBZ to the NBZ in the sense that

$$\Omega^{\text{occ}}(\mathbf{K}) = \sum_s \Omega^{\text{unf}}(\mathbf{k}_s), \quad (7)$$

which provides the link between Eqs. (4) and (5).

The difference between the unfolded SC curvature and the Berry curvature of the virtual crystal with averaged disorder reflects the disorder-mediated couplings between the folded bands, made possible by the relaxed crystal-momentum selection rule inside the SC. Such “pseudodirect” transitions⁴ modify the interband coherence effects described by Eq. (6), giving additional contributions to the anomalous velocity and AHC which are absorbed into the definition of $\Omega^{\text{unf}}(\mathbf{k})$.

A striking feature of the Berry curvature in crystalline ferromagnets is the occurrence of sharp peaks when two energy bands lying on either side of the Fermi level become quasi-degenerate.^{11,16,17} This can be understood in terms of Eq. (6) as a resonant enhancement behavior, and we will see that the same intuitive picture holds for the unfolded quantities: strong peaks in $\Omega^{\text{unf}}(\mathbf{k})$ can be traced back to pairs of unfolded bands separated by small (pseudo)direct gaps across ϵ_F .

III. BRILLOUIN-ZONE UNFOLDING

A. Basic definitions

Given a set of primitive translations $\{\mathbf{a}_i\}$ of the normal crystal cell (NC), the SC primitive translations can be written as $\sum_j M_{ij}\mathbf{a}_j$, with \mathbf{M} an integer matrix. Each point \mathbf{K} in the SBZ unfolds onto $|\mathbf{M}|$ distinct points $\mathbf{k}_s = \mathbf{K} + \mathbf{G}_s$ in the NBZ, where the \mathbf{G}_s are SC reciprocal lattice vectors.⁴

Following Ref. 3 we introduce a Bloch basis in the NBZ, and another in the SBZ. The basis states $|\mathbf{k}n\rangle$ and $|\mathbf{K}N\rangle$ are normalized over the NC and the SC respectively, and we define $\langle \dots \rangle$ as an integral over the SC volume, so that $\langle \mathbf{k}n | \mathbf{k}m \rangle = |\mathbf{M}| \delta_{n,m}$.

We also define the projection operator

$$\hat{T}(\mathbf{k}) = \frac{1}{|\mathbf{M}|} \sum_n |\mathbf{k}n\rangle \langle \mathbf{k}n|. \quad (8)$$

For any SC Bloch state we have $\sum_s \hat{T}(\mathbf{k}_s) |\mathbf{K}N\rangle = |\mathbf{K}N\rangle$, which simply means that the state $|\mathbf{K}N\rangle$ has unfolded Bloch character distributed among the points $\{\mathbf{k}_s\}$, with weights $\langle \mathbf{K}N | \hat{T}(\mathbf{k}_s) | \mathbf{K}N \rangle$ which add up to one.⁵

B. Unfolding a generic k -space quantity

Suppose we are interested in some property of the SC system which can be calculated in the SBZ as the trace of a Hermitian matrix

$$\mathcal{O}_{NM}(\mathbf{K}) = \langle \mathbf{K}N | \hat{\mathcal{O}} | \mathbf{K}M \rangle. \quad (9)$$

In order to map $\text{Tr } \mathcal{O}(\mathbf{K})$ from the SBZ onto the NBZ we first we set up the matrix elements of $\hat{\mathcal{O}}$ in the Bloch basis at the unfolded points,

$$\begin{aligned} \mathcal{O}_{nm}^{(u)}(\mathbf{k}_s) &= \frac{1}{|\mathbf{M}|} \langle \mathbf{k}_s n | \hat{\mathcal{O}} | \mathbf{k}_s m \rangle \\ &= \frac{1}{|\mathbf{M}|} \sum_{N,M} S_{nN}(\mathbf{k}_s, \mathbf{K}) \mathcal{O}_{NM}(\mathbf{K}) [S^\dagger(\mathbf{k}_s, \mathbf{K})]_{Mm}, \end{aligned} \quad (10)$$

where $S_{nN}(\mathbf{k}_s, \mathbf{K}) = \langle \mathbf{k}_s n | \mathbf{K}N \rangle$. Let us also define

$$\begin{aligned} T_{MN}(\mathbf{k}_s, \mathbf{K}) &= \langle \mathbf{K}M | \hat{T}(\mathbf{k}_s) | \mathbf{K}N \rangle \\ &= \frac{1}{|\mathbf{M}|} [S^\dagger(\mathbf{k}_s, \mathbf{K}) S(\mathbf{k}_s, \mathbf{K})]_{MN}, \end{aligned} \quad (11)$$

whose diagonal elements are the unfolding weights.

The unfolded quantity is given by the trace of Eq. (10),

$$\Omega^{\text{unf}}(\mathbf{k}_s) = \text{tr } \mathcal{O}^{(u)}(\mathbf{k}_s) = \text{Tr} [T(\mathbf{k}_s, \mathbf{K}) \mathcal{O}(\mathbf{K})], \quad (12)$$

where “tr” and “Tr” denote traces over the NC and SC orbital indices n and N respectively. Equation (12) is our basic prescription for BZ unfolding. In Appendix A we verify that it correctly gives the unfolded energy bands.

1. Gauge invariance of unfolded quantities

Under a unitary mixing of the SC basis states,

$$|\mathbf{K}N\rangle \rightarrow \sum_M |\mathbf{K}M\rangle U_{MN}(\mathbf{K}), \quad (13)$$

the matrix (11) changes in a gauge-covariant manner,

$$T(\mathbf{k}_s, \mathbf{K}) \rightarrow U^\dagger(\mathbf{K}) T(\mathbf{k}_s, \mathbf{K}) U(\mathbf{K}). \quad (14)$$

If the matrix $\mathcal{O}(\mathbf{K})$ is also gauge-covariant, then Eq. (12) remains unchanged under the transformation. This gauge-invariance requirement will dictate which definition of a “Berry curvature matrix” to use for unfolding purposes. (While the matrix representation (9) of most quantities is unique and trivially gauge-covariant, the Berry curvature is more subtle, as it involves k -space derivatives of the state vectors.)

C. Unfolded Berry curvature

Our goal is to unfold the Berry curvature of the SC system from the SBZ to the NBZ. Since the unfolding

formalism developed above is based on matrix objects, we begin by defining a Hermitean Berry curvature matrix $\Omega_{ab,NM}(\mathbf{K}) = \Omega_{ab,MN}^*(\mathbf{K})$ satisfying two essential requirements: (i) it should be gauge-covariant in the sense of Eq. (14), and (ii) its trace should give the quantity to be unfolded: $\text{Tr} \Omega_{ab}(\mathbf{K}) = \Omega_{ab}^{\text{occ}}(\mathbf{K})$.

Those requirements are fulfilled by the non-Abelian Berry curvature matrix.^{2,18} For an insulator it reads

$$\Omega_{ab,NM} = \partial_a A_{b,NM} - \partial_b A_{a,NM} - i[A_a, A_b]_{NM}, \quad (15)$$

where \mathbf{K} has been dropped everywhere for brevity. Here $\partial_a = \partial/\partial K_a$, $A_{a,NM} = i\langle u_N | \partial_a u_M \rangle$ is the Berry connection matrix, and the indices N, M run over the occupied states. Except for the commutator, Eq. (15) is the obvious matrix generalization of Eq. (3). The extra term does not affect the trace, but is needed to ensure gauge-covariance.

For our purposes it will be convenient to recast Eq. (15) in terms of projection operators,¹⁸

$$\Omega_{ab,NM} = iF_{ab,NM} - iF_{ba,NM}, \quad (16)$$

where

$$F_{ab,NM} = \langle u_N | (\partial_a \hat{P}) \hat{Q} (\partial_b \hat{P}) | u_M \rangle = F_{ba,MN}^* \quad (17)$$

and \hat{P} , $\hat{Q} = \hat{1} - \hat{P}$ span the occupied and unoccupied spaces respectively. Metals can be handled by writing

$$\hat{P} = \sum_{N,M} |u_N\rangle f_{NM} \langle u_M|, \quad (18)$$

where f_{NM} is the occupation matrix.¹⁹ For insulators $\hat{P} = \sum_N^{\text{occ}} |u_N\rangle \langle u_N|$, and a few lines of algebra show that Eq. (16) reduces to Eq. (15).

With these definitions, the Berry curvatures in the original SBZ and unfolded onto the NBZ via Eq. (12) read

$$\Omega_{ab}^{\text{occ}}(\mathbf{K}) = -2\text{Im} \text{Tr} F_{ab}(\mathbf{K}) \quad (19)$$

$$\Omega_{ab}^{\text{unf}}(\mathbf{k}_s) = -2\text{Im} \text{Tr} [T(\mathbf{k}_s, \mathbf{K}) F_{ab}(\mathbf{K})]. \quad (20)$$

Equation (19) was given in Ref. 18, while Eq. (20) is a primary result of the present work.

It is easily verified (see Appendix B) that Eq. (20) satisfies the sum rule (7), which allows to recast the geometric AHC of the SC system as an integral over the NBZ according to Eqs. (4) and (5).

D. Implementation in a Wannier basis

In this section we describe the implementation of Eq. (20) using Wannier interpolation, which is carried out as a post-processing step following a first-principles SC calculation. Essentially, we combine two Wannier-based

methodologies: that of Refs. 17 and 19 for computing the Berry curvature, and that of Ref. 3 for BZ unfolding.

In the formalism of Ref. 3 the Bloch basis orbitals are chosen as $|\mathbf{K}N\rangle = \sum_{\mathbf{R}} e^{i\mathbf{K}\cdot\mathbf{R}} |\mathbf{R}N\rangle$, where $|\mathbf{R}N\rangle$ is a Wannier function and \mathbf{R} a SC lattice vector. The Wannier functions are then mapped onto the NC according to $|\mathbf{R}N\rangle \leftrightarrow |r n\rangle = |\mathbf{R} + [\mathbf{r}], n\rangle$, with a choice of $|\mathbf{M}|$ NC lattice vectors $[\mathbf{r}]$ such that no two $[\mathbf{r}]$'s differ by an \mathbf{R} . Once a map has been chosen, any NC lattice vector \mathbf{r} can be uniquely decomposed as $\mathbf{r} = \mathbf{R} + [\mathbf{r}]$. Setting $|\mathbf{k}n\rangle = \sum_{\mathbf{r}} e^{i\mathbf{k}\cdot\mathbf{r}} |r n\rangle$ then gives³

$$S_{nN}(\mathbf{k}_s, \mathbf{K}) = \langle \mathbf{k}_s n | \mathbf{K} N \rangle = e^{-i\mathbf{k}_s \cdot [\mathbf{r}](N)} \delta_{n,n'(N)}, \quad (21)$$

which goes into the unfolding equations (11) and (12).

The expression for the unfolded Berry curvature involves several other matrix objects, which we now define borrowing the notation from Ref. 19. The two basic objects are (omitting orbital indices)

$$\mathbb{H}(\mathbf{K}) = \sum_{\mathbf{R}} e^{i\mathbf{K}\cdot\mathbf{R}} \langle \mathbf{0} | \hat{H} | \mathbf{R} \rangle \quad (22)$$

$$\mathbb{A}_a(\mathbf{K}) = \sum_{\mathbf{R}} e^{i\mathbf{K}\cdot\mathbf{R}} \langle \mathbf{0} | \hat{x}_a | \mathbf{R} \rangle. \quad (23)$$

Diagonalization of $\mathbb{H}(\mathbf{K})$ gives the energy eigenvalues,

$$\mathbb{H}_{JJ'}^{(\text{H})}(\mathbf{K}) = [U^\dagger(\mathbf{K}) \mathbb{H}(\mathbf{K}) U(\mathbf{K})]_{JJ'} = \epsilon_{\mathbf{K}J} \delta_{JJ'}, \quad (24)$$

where the superscript (H) stands for ‘‘Hamiltonian gauge.’’ Next we define

$$J_{a,JJ'}^{(\text{H})}(\mathbf{K}) = \begin{cases} \frac{i \{U^\dagger(\mathbf{K}) [\partial_a \mathbb{H}(\mathbf{K})] U(\mathbf{K})\}_{JJ'}}{\epsilon_{\mathbf{K}J'} - \epsilon_{\mathbf{K}J}} & \text{if } J' \neq J \\ 0 & \text{if } J' = J \end{cases} \quad (25)$$

and $J_a = U J_a^{(\text{H})} U^\dagger$. This matrix will only appear in the combinations $J_a^+ = f J_a g$ and $J_a^- = g J_a f$, where f is the occupation matrix introduced in Eq. (18), and $g = 1 - f$. With these definitions, the unfolded curvature in the Wannier basis becomes (see derivation in Appendix C)

$$\begin{aligned} \Omega_{ab}^{\text{unf}}(\mathbf{k}_s) = & \text{Re} \text{Tr} [T f (\partial_a \mathbb{A}_b - \partial_b \mathbb{A}_a) f] \\ & + 2\text{Im} \text{Tr} [T f \mathbb{A}_a f \mathbb{A}_b f] \\ & - 2\text{Im} \text{Tr} [T (f \mathbb{A}_a J_b^+ + J_a^- \mathbb{A}_b f + J_a^- J_b^+)]. \end{aligned} \quad (26)$$

Equation (26) is our second important result. It expresses the unfolded Berry curvature at a point \mathbf{k}_s in the NBZ in terms of the matrix $T(\mathbf{k}_s, \mathbf{K})$ given by Eqs. (11) and (21), and additional matrices defined at the folded point \mathbf{K} in the SBZ. Those other matrices can be computed from a knowledge of the Hamiltonian and position-operator matrix elements in the Wannier basis, which are then Fourier transformed into $\mathbb{H}(\mathbf{K})$ and $\mathbb{A}_a(\mathbf{K})$ via Eqs. (22) and (23). Diagonalization of $\mathbb{H}(\mathbf{K})$ [Eq. (24)] provides the energy eigenvalues and rotation matrices

used to compute $f(\mathbf{K})$ and $J_a^\pm(\mathbf{K})$.¹⁹ Note that the needed derivatives $\partial_a \mathbb{H}(\mathbf{K})$ and $\partial_b \mathbb{A}_a(\mathbf{K})$ are easily obtained by differentiating Eqs. (22) and (23).

It is instructive to consider the trivial unfolding scenario where the NC and the SC are the same. Then T becomes the identity matrix, the second term in Eq. (26) vanishes since $\text{Im Tr}[\mathbb{A}_a f \mathbb{A}_b f] = 0$, and $\mathbf{\Omega}^{\text{unf}}(\mathbf{k})$ correctly reduces to Eq. (51) of Ref. 19 for $\mathbf{\Omega}^{\text{occ}}(\mathbf{k})$.

IV. COMPUTATIONAL DETAILS

Plane-wave pseudopotential calculations were carried out for bcc Fe, bcc Co, and an Fe–Co ordered alloy with the Fe_3Al structure.²⁰ The experimental lattice constant $a = 5.42$ bohr of bcc Fe was used in all cases to facilitate comparisons, and the magnetization was set along the [001] direction.

The calculations were performed with the `Pwscf` code from the `Quantum-Espresso` package,²¹ in a noncollinear spin framework with fully relativistic norm-conserving pseudopotentials generated from parameters similar to those in Ref. 17. An energy cutoff of 120 Ry was used for the plane-wave expansion of the wavefunctions, and exchange and correlation effects were treated within the PBE generalized-gradient approximation.²²

In the case of bcc Fe and bcc Co, the self-consistent total energy calculations were done with a $16 \times 16 \times 16$ Monkhorst-Pack mesh for the BZ integration, while for the non-self-consistent calculation a $10 \times 10 \times 10$ mesh was used, and the 28 lowest bands were calculated. In the case of Fe_3Co the BZ integration meshes were $12 \times 12 \times 12$ and $10 \times 10 \times 10$ for the self-consistent and bandstructure calculations respectively, and the 112 lowest bands were calculated. A Fermi smearing of 0.02 Ry was used in all self-consistent calculations.

For each material, eighteen spinor Wannier functions per atom were then constructed using `Wannier90`.²³ Atom-center s , p , and d -like trial orbitals were used for the initial projection step, followed by an iterative procedure to select an optimal “disentangled” subspace,²⁴ using the same inner and outer energy windows as in Ref. 17. At variance with that work, no minimization of the spread functional was done to further improve the localization properties of the “projected” Wannier functions.²⁵ This was done to keep the Wannier functions of Fe_3Co as similar as possible to those of bcc Fe, as required by the Wannier-based unfolding scheme.³

In the next section we show results for the energy bands and Berry curvature of the Fe_3Co ordered alloy unfolded onto the NBZ of bcc Fe. For comparison purposes, we also show the energy bands and Berry curvatures of pure Fe and of the VCA alloy computed directly in the NBZ. Following Ref. 9, we have implemented the VCA in the basis of projected Wannier functions, by linearly mixing the Hamiltonian matrix elements of bcc Fe and bcc Co. Since the Wannier interpolation of the Berry curvature also requires the position-operator matrix elements,¹⁷ we

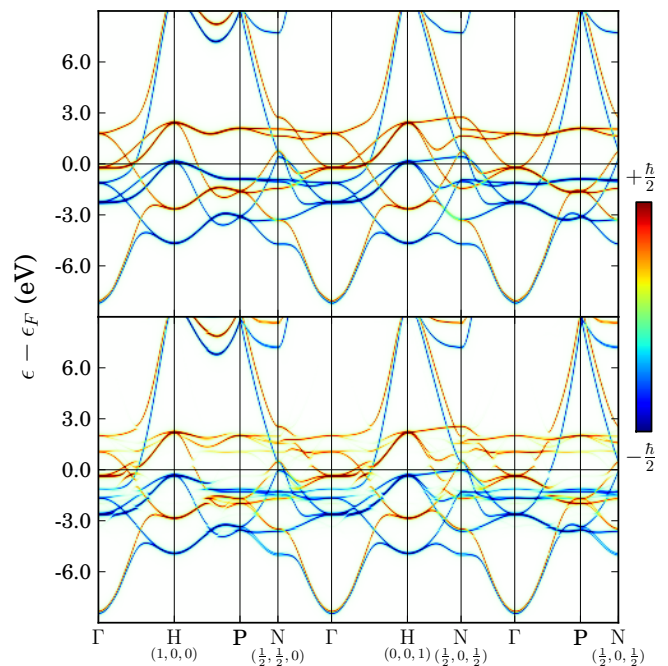


FIG. 1. (Color online.) Upper panel: Energy bands of bcc Fe. Lower-panel: Energy bands of the fcc Fe_3Co alloy unfolded onto the Brillouin zone of bcc Fe. Colors indicate the spin polarization $\langle S_z \rangle$ of the states. The points labelled P all have coordinates $(1/2, 1/2, 1/2)$. The bands of the bcc $\langle \text{Fe}_3\text{Co} \rangle$ virtual crystal (not shown) are almost indistinguishable from those of bcc Fe, except for a shift in the Fermi level.

modified them accordingly.

In all cases, with and without unfolding, we plot the Bloch spectral function instead of the energy bands. To generate the plots we use the method of Ref. 7, adapted to display the spin polarization $\langle S_z \rangle$ as a color code. A similar procedure is used to plot the intersections of the (unfolded) Fermi surface with a plane in the NBZ. For simplicity, we will continue to use the expressions “energy bands” and “Fermi surface intersections” (or “Fermi lines”) when referring to the figures.

V. RESULTS

We have selected Fe–Co, a substitutional alloy based on the bcc structure, as a test case for the Berry curvature unfolding procedure. We focus on a composition of 25% Co, using the Fe_3Al ordered structure as a representative configuration.²⁰ This structure is of the Heusler X_2YZ type, with $X=Y=\text{Fe}$ and $Z=\text{Co}$ (pure bcc Fe corresponds to $X=Y=Z=\text{Fe}$). The Bravais lattice is fcc with a four-atom basis, so that the energy bands live in a folded BZ which is four times smaller than the NBZ of bcc Fe. This makes a direct comparison with the bandstructure of bcc Fe rather difficult, and typically only the densities of states are compared.²⁰

Information about the k -space distribution of the elec-

tron states in the alloy can be recovered by plotting the energy bands unfolded onto the NBZ [Eq. (A3)]. The result, shown in the lower panel of Fig. 1, strongly resembles the bands of bcc Fe in the upper panel. The influence of the Co atoms is clearly visible in certain regions of the (\mathbf{k}, E) plane, in the form of “broken bands” and “ghost bands.” Overall, the effects of alloying are most pronounced for the narrow d bands crossing the Fermi level.

We now turn to the k -space Berry curvature, Eqs. (2) and (6), and begin by recalling its salient features in crystalline metallic ferromagnets.^{11,16,17} In this class of materials the Berry curvature is induced by the combined effect of exchange splitting and spin-orbit coupling, which together break time-reversal symmetry in the orbital wavefunctions. $\Omega^{\text{occ}}(\mathbf{k})$ is characterized by strong, sharp features which are concentrated around the Fermi surface, in regions where occupied and empty bands come in close contact and become strongly coupled by spin-orbit. This is illustrated for bcc Fe in Fig. 2(a), which displays the energy bands near the Fermi level and the Berry curvature, along the Γ -H-P path. The spiky features rise above a smooth, low-intensity background which is visible in the heatmap plot of the Berry curvature over the $k_y = 0$ plane, Fig. 3(a).

In order to understand how alloying with Co disturbs the Berry curvature, we first consider the effects in the virtual-crystal approximation, that is, for a bcc crystal composed of “averaged” $\langle \text{Fe}_3\text{Co} \rangle$ atoms. Since \mathbf{k} remains a good quantum number in the NBZ, the energy bands and Berry curvature can be obtained in the usual manner (without unfolding), and are shown in Fig. 2(b). The bands are quite similar to those of bcc Fe, and the main effect of alloying is an upward shift of the Fermi level. This leads to significant changes in the Berry curvature: for example, the strong peak along H-P is completely suppressed, since the two majority bands involved are now both occupied. Only some very low-intensity features remain along Γ -H (note the difference in the Berry curvature scales between the panels in Fig. 2).

Comparing the heatmaps in Figs. 3(a,b) we again see significant differences in the Berry curvature distribution, due to the shift in the Fermi level across narrow d bands. In both cases the Berry curvature is concentrated in regions where there are weak avoided crossings between two Fermi lines, which can be of opposite-spin character or of like-spin character.

Missing from the VCA description of the alloy are the effects brought about by the reduced translational order, which are the main focus of this work. Their influence on the bandstructure was revealed by plotting the unfolded bands of fcc Fe_3Co in Fig. 1. In order to see how the the Berry curvature is affected, we plot together in Fig. 2(c) the two unfolded quantities, energy bands and Berry curvature.

Compared to the VCA results in Fig. 2(b) the Fermi level has not moved appreciably, and the bigger changes are in the bands themselves, especially in the minority

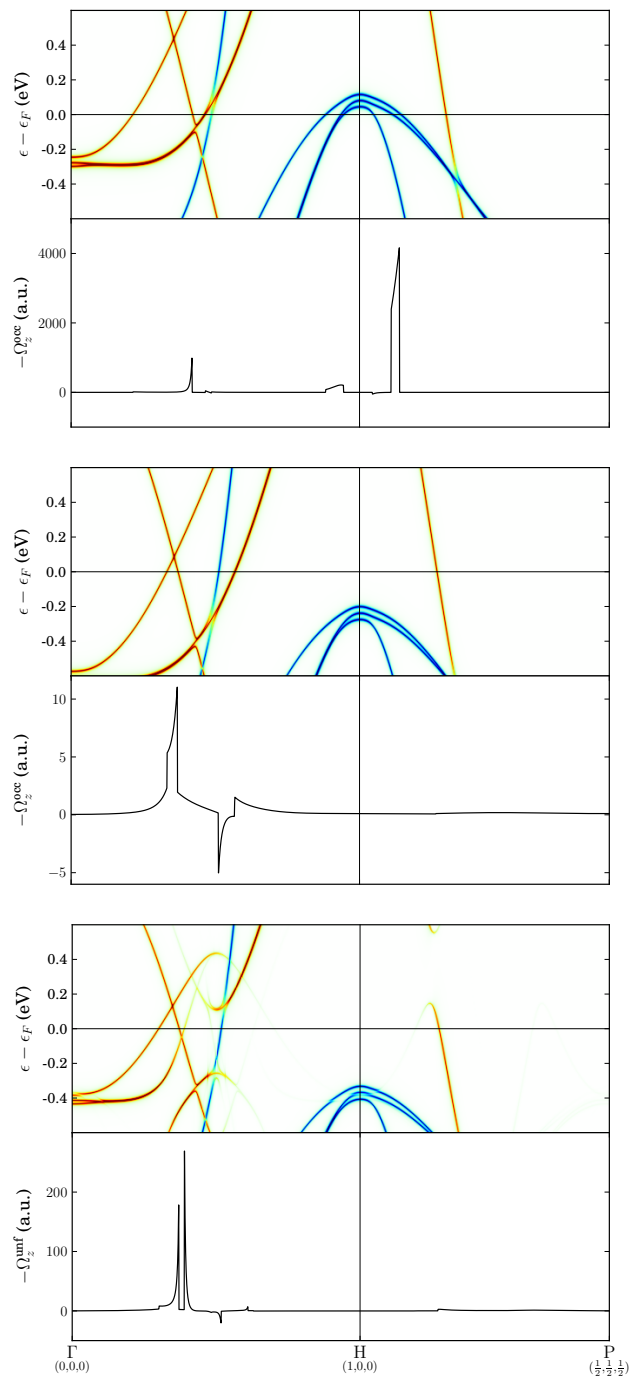


FIG. 2. (Color online.) Energy bands color-coded by the spin polarization $\langle S_z \rangle$ and Berry curvature summed over the occupied states, plotted along the path Γ -H-P. Upper panel: bcc Fe. Middle panel: bcc $\langle \text{Fe}_3\text{Co} \rangle$ virtual crystal. Lower panel: fcc Fe_3Co alloy, using BZ unfolding.

states near the Fermi level. The Berry curvature displays two contiguous strong peaks along Γ -H. They are associated with spectral features which have been greatly modified with respect to the VCA calculation, namely, a pair of minority bands with a weak avoided crossing just below the Fermi level. As the upper band rises above

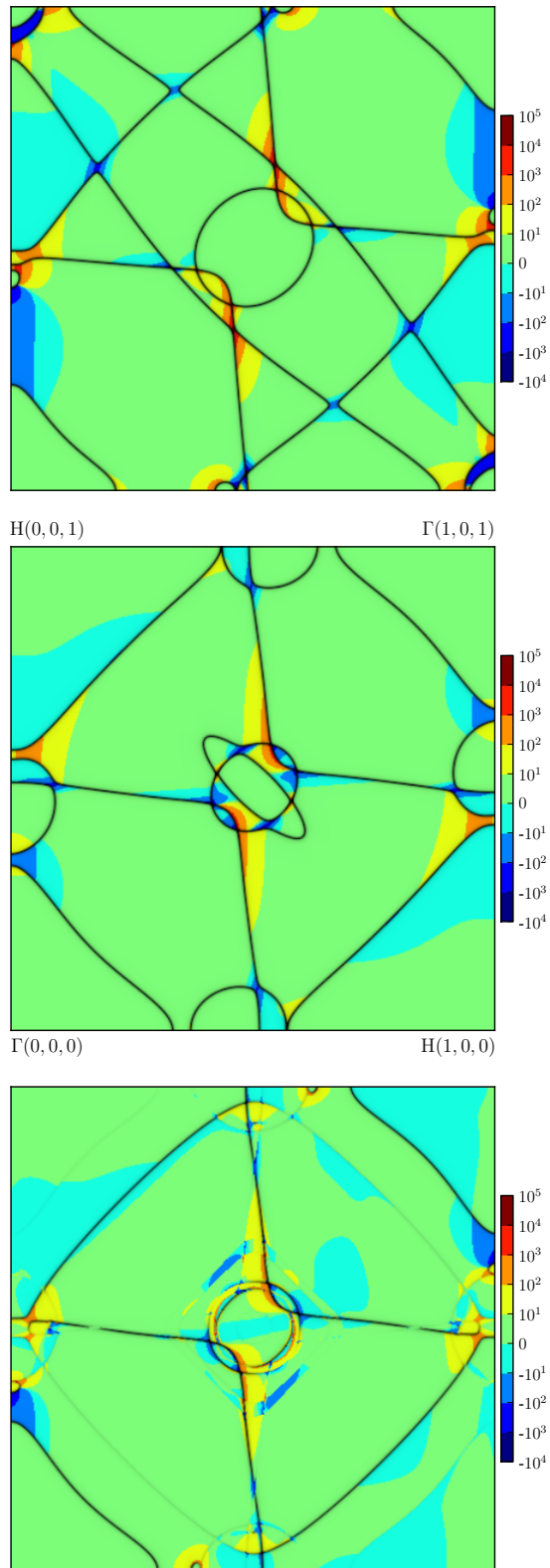


FIG. 3. (Color online.) Heatmap of the Berry curvature in the plane $k_y = 0$, in atomic units (note the log scale). The lines of intersection between the Fermi surface and the plane are also shown. The upper and middle panels show $-\Omega_z^{\text{occ}}$ for bcc Fe and bcc $\langle\text{Fe}_3\text{Co}\rangle$ respectively, and the lower panel shows $-\Omega_z^{\text{unf}}$ for fcc Fe_3Co .

ϵ_F on either side of the crossing, a Berry-curvature peak suddenly develops and then quickly drops as the separation between the two bands increases. Plots along other high-symmetry lines in the NBZ show similar features. We conclude that the intuitive “interband coupling” interpretation of the Berry curvature based on Eq. (6) carries over to the unfolded curvature, now in terms of the unfolded bands. Further confirmation of this comes from inspecting the unfolded Fermi lines and Berry curvature across the $k_y = 0$ plane in Fig. 3(c). Overall they resemble those of the VCA crystal, but with some distortions. As before, the Berry curvature is concentrated in regions where two Fermi lines approach one another.

To conclude we evaluate the AHC of the three systems from Eqs. (1) and (4). The results were carefully converged with respect to k -point sampling,^{16,17} using dense uniform meshes which were adaptively refined around points where the Berry curvature exceeded a threshold magnitude of 27.98 \AA^2 . Uniform (adaptive) meshes of up to $350 \times 350 \times 350$ ($13 \times 13 \times 13$) in the NBZ were used for Fe and $\langle\text{Fe}_3\text{Co}\rangle$. For Fe_3Co the densest uniform (adaptive) mesh in the SBZ was $250 \times 250 \times 250$ ($11 \times 11 \times 11$). The converged AHC values are 758 S/cm for bcc Fe, 452 S/cm for bcc $\langle\text{Fe}_3\text{Co}\rangle$, and 473 S/cm for fcc Fe_3Co . We will comment on these numbers shortly.

VI. DISCUSSION AND OUTLOOK

As illustrated by our calculations, impurities modify the interband couplings responsible for the intrinsic AHC in perfectly ordered crystals. In the context of SC calculations it is very natural to combine the putative intrinsic contribution of Eq. (1) with those disorder corrections into a single geometric contribution, Eq. (4), which is a gauge-invariant property of the disordered electronic ground state. In Chern insulators, where the AHE is quantized for topological reasons (QAHE), the disorder corrections cancel out upon taking the integral in Eq. (4). In metals the AHE is not quantized, and disorder gives a net geometric contribution on top of the intrinsic one.

In the same way that the intrinsic AHC can be viewed as the dc limit of the interband conductivity of the pristine crystal,¹ the geometric AHC corresponds to the dc limit of the interband conductivity of a SC with disorder, whose “bands” are defined in the folded BZ. For disordered systems possessing a parent ordered structure, the familiar representation in terms of a Berry curvature in the normal BZ can be partially restored by means of the unfolded Berry curvature (20), leading to Eq. (5) which has the same form as Eq. (1).

In pristine crystals the geometric AHC reduces to the intrinsic contribution. It therefore retains the essential features of the intrinsic theory of the AHE, while at the same time addressing the main criticism that it originally faced, namely, “the complete absence of scattering from disorder in the derived Hall response contribution.”¹

Given the reasonably good agreement with experiment

which has been achieved from first principles calculations based on Eq. (1), one should be cautious about introducing modifications. The calculations presented in this work are reassuring in that regard: most of the large change in the calculated AHC between pure bcc Fe and the Fe–Co alloy is recovered at the VCA “intrinsic” level from the band-filling effect, while “scattering” effects from the reduced translational order in the fcc cell give some corrections, without dramatically changing the result. The same conclusion can be drawn from comparing Figs. 3(b,c).

The system we have studied is of course a very crude model for a real disordered alloy. Calculations using larger SCs with more realistic descriptions of disorder will be needed to make detailed comparisons between the (unfolded) Berry curvature of a disordered crystal or alloy and that of the parent crystal. For example, it seems plausible that disorder-induced contributions will be smoothed out compared to the sharp features seen in Figs. 2(c) and 3(c). The Wannier-based SC methodology of Ref. 7 seems particularly well-suited for such studies.

It would be desirable to clarify which scattering contributions are included in the geometric AHC. We give a discussion based on the Kubo-Greenwood (KG) formula for the SC system,²⁶ written here for $\omega = 0$:

$$\sigma_{ab} = \frac{ie^2}{NV} \sum_{\mathbf{K}, J, J'} \frac{f_{J'} - f_J}{\epsilon_{J'} - \epsilon_J} \frac{\langle J | \hat{v}_a | J' \rangle \langle J' | \hat{v}_b | J \rangle}{\epsilon_{J'} - \epsilon_J - i\eta}, \quad (27)$$

where V is the SC volume and the SBZ is sampled over N points \mathbf{K} . The full AHC, the sum of intrinsic, skew-scattering, and side-jump contributions, can be calculated as the antisymmetric part of Eq. (27). Let us recall the role played by the parameter η : for a finite volume V the energy levels at fixed \mathbf{K} are discrete, and absorption becomes impossible at frequencies smaller than the level spacing. It is for this reason that in SC calculations of the residual resistivity $\rho_{xx} = 1/\sigma_{xx}$ one must use a level broadening $\eta(V)$ greater than the mean level spacing at ϵ_F .²⁷ Similar considerations should be relevant for σ_{xy} , particularly when trying to recover the skew-scattering contribution, which scales as σ_{xx} and has a similar physical origin.¹

This analysis suggests that $\sigma_{xy}^{\text{geom}}$, which is obtained from Eq. (27) by taking the $\eta \rightarrow 0^+$ limit at finite V , does not include skew-scattering. Since the longitudinal conductivity σ_{xx} vanishes in that limit, $\sigma_{xy}^{\text{geom}}$ corresponds to the *dissipationless* part of σ_{xy} , and this is precisely how the sum of the intrinsic and side-jump contributions is defined¹ and measured.²⁸

Leaving aside matters of definition and interpretation, our gauge-invariant procedure for unfolding the Berry curvature from SC calculations seems useful in its own right as an analysis tool complementary to the unfolding of energy bands. The k -space Berry curvature induced by interband coherence effects has emerged as a powerful paradigm to describe the AHE,^{1,2} and the methods de-

veloped in this work seamlessly incorporate disorder into the picture.

In closing, we mention that the BZ unfolding procedure can be readily applied to other k -space quantities which take the form of traces over gauge-covariant matrices. Examples include the occupation numbers $n(\mathbf{K}) = \text{Tr} f(\mathbf{K})$, the integrand of the k -space orbital magnetization formula,^{18,19} and the quantum metric.²⁵

ACKNOWLEDGMENTS

This work was supported by grants No. MAT2012-33720 from the Ministerio de Economía y Competitividad (Spain), No. CIG-303602 from the European Commission, and by ONR Grant No. N00014-12-1-1041 (USA).

Appendix A: Unfolded energy bands

The spectral operator $(E + i\eta - \hat{H})^{-1}$ projected onto the Bloch space at \mathbf{K} reads, in the SC eigenstate basis,

$$\hat{G}_{\mathbf{K}}(E + i\eta) = \sum_J \frac{|\mathbf{K}J\rangle\langle\mathbf{K}J|}{E + i\eta - \epsilon_{\mathbf{K}J}}. \quad (A1)$$

The \mathbf{K} -resolved density of states (Bloch spectral function) consists of sharp peaks in the SBZ, corresponding to the “folded” energy bands:

$$\begin{aligned} D_{\mathbf{K}}(E) &= -\frac{1}{\pi} \lim_{\eta \rightarrow 0^+} \text{Im Tr } G_{\mathbf{K}}(E + i\eta) \\ &= \sum_J \delta(E - \epsilon_{\mathbf{K}J}). \end{aligned} \quad (A2)$$

Applying the unfolding prescription of Eq. (12) to the operator $\hat{O} = (-1/\pi)\hat{G}_{\mathbf{K}}(E + i\eta)$ we find

$$\begin{aligned} D_{\mathbf{k}_s}^{\text{unf}}(E) &= \lim_{\eta \rightarrow 0^+} \text{Im tr } \mathcal{O}^{(u)}(\mathbf{k}_i) \\ &= \sum_J T_{JJ}(\mathbf{k}_s, \mathbf{K}) \delta(E - \epsilon_{\mathbf{K}J}). \end{aligned} \quad (A3)$$

This is the known expression for the unfolded Bloch spectral function,³ with

$$T_{JJ}(\mathbf{k}_s, \mathbf{K}) = \frac{1}{|\mathbf{M}|} \sum_n |\langle \mathbf{k}_s n | \mathbf{K}J \rangle|^2 \quad (A4)$$

the spectral weight of $|\mathbf{K}J\rangle$ at \mathbf{k}_s . (The factor of $1/|\mathbf{M}|$ on the right-hand-side is absent when adopting the normalization convention of Ref. 3.)

Appendix B: Unfolding sum rule

As mentioned in Sec. III A, the unfolding weights satisfy $\sum_s T_{NN}(\mathbf{k}_s, \mathbf{K}) = 1$. To find the resulting sum rule

for $\mathcal{O}^{\text{unf}}(\mathbf{k})$, evaluate Eq. (12) in a basis where either $T(\mathbf{k}_s, \mathbf{K})$ or $\mathcal{O}(\mathbf{K})$ is diagonal, and sum over \mathbf{k}_s :

$$\sum_{s=1}^{|\mathbf{M}|} \mathcal{O}^{\text{unf}}(\mathbf{k}_s) = \sum_{s=1}^{|\mathbf{M}|} \sum_N T_{NN}(\mathbf{k}_s, \mathbf{K}) \mathcal{O}_{NN}(\mathbf{K}) = \text{Tr } \mathcal{O}(\mathbf{K}). \quad (\text{B1})$$

(This corresponds to Eq. (7) for the Berry curvature.) Now sum over a uniform grid in the SBZ, replace $\sum_{\mathbf{K}}^{\text{SBZ}} \sum_s$ on the left-hand side with $\sum_{\mathbf{k}}^{\text{NBZ}}$, and take the continuum limit to find

$$\int_{\text{NBZ}} d^3k \mathcal{O}^{\text{unf}}(\mathbf{k}) = \int_{\text{SBZ}} d^3K \text{Tr } \mathcal{O}(\mathbf{K}), \quad (\text{B2})$$

which corresponds to Eqs. (4) and (5).

Appendix C: Derivation of Eq. (26)

In this Appendix we derive Eq. (26) for $\Omega_{ab}^{\text{unf}}(\mathbf{k}_s)$ starting from Eq. (20). Following Ref. 19, we adopt a notation where matrix objects written with a double staff, such as $\mathbb{A}_{NM}(\mathbf{K}) = i\langle u_{\mathbf{K}N} | \partial_a u_{\mathbf{K}M} \rangle$ in Eq. (23), are defined

over the space spanned by the Wannier functions, which for metals typically contains some low-lying empty states in addition to all the occupied states.²⁴ Instead, objects with a single staff such as $A_{NM}(\mathbf{K})$ in Eq. (15) are defined over the occupied subspace. So, for example, we define (dropping \mathbf{K} everywhere) $\hat{\mathbb{P}} = \sum_N |u_N\rangle\langle u_N|$, $\hat{\mathbb{Q}} = \hat{1} - \hat{\mathbb{P}}$, and $\mathbb{F}_{ab, NM} = i\langle \partial_a u_N | \hat{\mathbb{Q}} | \partial_b u_M \rangle$ as counterparts to \hat{P} , \hat{Q} , and $F_{ab, NM}$ in Eqs. (17) and (18).

We further condense our notation by dropping indices N, M , e.g., $\mathbb{P} = |u\rangle\langle u|$ and $\hat{P} = |u\rangle f\langle u|$. We will use the relations¹⁹

$$(\partial_a \hat{P}) \hat{Q} = |u\rangle f\langle \partial_a u | \hat{\mathbb{Q}} + i|u\rangle f(\mathbb{A}_a + J_a)g\langle u| \quad (\text{C1})$$

and (compare with Eqs. (15) and (16))

$$i\mathbb{F}_{ab} - i\mathbb{F}_{ba} = \partial_a \mathbb{A}_b - \partial_b \mathbb{A}_a - i[\mathbb{A}_a, \mathbb{A}_b]. \quad (\text{C2})$$

Expanding Eq. (17) with the help of Eq. (C1) we find

$$F_{ab} = f\mathbb{F}_{ab}f + f\mathbb{A}_a g \mathbb{A}_b f + J_a^- \mathbb{A}_b f + f\mathbb{A}_a J_b^+ + J_a^- J_b^+. \quad (\text{C3})$$

Writing Eq. (20) as $\Omega_{ab}^{\text{unf}} = i\text{Tr} \{T[F_{ab} - F_{ba}]\}$, inserting Eq. (C3) and then using Eq. (C2), we arrive at Eq. (26).

-
- ¹ N. Nagaosa, J. Sinova, S. Onoda, A. H. MacDonald, and N. P. Ong, Rev. Mod. Phys. **82**, 1539 (2010).
² D. Xiao, M.-C. Chang, and Q. Niu, Rev. Mod. Phys. **82**, 1959 (2010).
³ W. Ku, T. Berlijn, and C.-C. Lee, Phys. Rev. Lett. **104**, 216401 (2010).
⁴ V. Popescu and A. Zunger, Phys. Rev. B **85**, 085201 (2012).
⁵ P. B. Allen, T. Berlijn, D. A. Casavant, and J. M. Soler, Phys. Rev. B **87**, 085322 (2013).
⁶ S. Baroni, S. de Gironcoli, and P. Giannozzi, Phys. Rev. Lett. **65**, 84 (1990).
⁷ T. Berlijn, D. Volja, and W. Ku, Phys. Rev. Lett. **106**, 077005 (2011).
⁸ T. Berlijn, P. J. Hirschfeld, and W. Ku, Phys. Rev. Lett. **109**, 147003 (2012).
⁹ J. Liu and D. Vanderbilt, Phys. Rev. B **88**, 224202 (2013).
¹⁰ S. Lowitzer, D. Ködderitzsch, and H. Ebert, Phys. Rev. Lett. **105**, 266604 (2010).
¹¹ Z. Fang, N. Nagaosa, K. Takahashi, A. Asamitsu, R. Matthieu, T. Ogasawara, H. Yamada, M. Kawasaki, Y. Tokura, and K. Terakura, Science **302**, 92 (2003).
¹² Y. Yao, Y. Liang, D. Xiao, Q. Niu, S.-Q. Shen, X. Dai, and Z. Fang, Phys. Rev. B **75**, 020401 (2007).
¹³ T. Jungwirth, Q. Niu, and A. H. MacDonald, Phys. Rev. Lett. **88**, 207208 (2002).
¹⁴ E. Prodan, T. L. Hughes, and B. A. Bernevig, Phys. Rev. Lett. **105**, 115501 (2010).
¹⁵ Y.-F. Zhang, Y.-Y. Y. and Y. Ju, L. Sheng, R. Shen, D.-N. Sheng, and D.-Y. Xing, Chinese Phys. B **22**, 117312 (2013).
¹⁶ Y. Yao, L. Kleinman, A. H. MacDonald, J. Sinova, T. Jungwirth, D.-S. Wang, E. Wang, and Q. Niu, Phys. Rev. Lett. **92**, 037204 (2004).
¹⁷ X. Wang, J. R. Yates, I. Souza, and D. Vanderbilt, Phys. Rev. B **74**, 195118 (2006).
¹⁸ D. Ceresoli, T. Thonhauser, D. Vanderbilt, and R. Resta, Phys. Rev. B **74**, 024408 (2006).
¹⁹ M. G. Lopez, D. Vanderbilt, T. Thonhauser, and I. Souza, Phys. Rev. B **85**, 014435 (2012).
²⁰ K. Schwarz, P. Mohn, and J. Kübler, J. Phys. F: Met. Phys. **14**, 2659 (1984).
²¹ P. Giannozzi *et al.*, J. Phys. Condens. Matter **21**, 395502 (2009).
²² J. P. Perdew, K. Burke, and M. Ernzerhof, Phys. Rev. Lett. **77**, 3865 (1996).
²³ A. A. Mostofi, J. R. Yates, Y.-S. Lee, I. Souza, D. Vanderbilt, and N. Marzari, Comput. Phys. Commun. **178**, 685 (2008).
²⁴ I. Souza, N. Marzari, and D. Vanderbilt, Phys. Rev. B **65**, 035109 (2001).
²⁵ N. Marzari and D. Vanderbilt, Phys. Rev. B **56**, 12847 (1997).
²⁶ A. Shitade and N. Nagaosa, J. Phys. Soc. Japan **81**, 083704 (2012).
²⁷ R. H. Brown, P. B. Allen, D. M. Nicholson, and W. H. Butler, Phys. Rev. Lett. **62**, 661 (1989).
²⁸ Y. Tian, L. Ye, and X. Jin, Phys. Rev. Lett. **103**, 087206 (2009).